JOURNAL OF GEOPHYSICAL RESEARCH, VOL. 101, NO. D13, PAGES 18,793–18,806, AUGUST 20, 1996

Algorithm for the estimation of vertical ozone profiles from the backscattered ultraviolet technique

P. K. Bhartia,[1] R. D. McPeters,[1] C. L. Mateer,[2] L. E. Flynn,[3] and C. Wellemeyer[4]

Abstract. An implementation of the optimal estimation scheme to obtain vertical ozone profiles from satellite measurements of backscattered solar ultraviolet (buv) radiation is described. This algorithm (Version 6.0) has been used to produce a 15-year data set of global ozone profiles from Nimbus 7 SBUV, NOAA 11 SBUV/2, and Space Shuttle SSBUV instruments. A detailed discussion of the information content of the measurement is presented. Using high vertical resolution ozone profiles from the SAGE II experiment as "truth" profiles, it is shown that the buv technique can capture short-term variabilities of ozone in 5-km vertical layers, between 0.3 mbar and 100 mbar, with a precision of 5–15%. However, outside the 1–20 mbar range, buv-derived results are heavily influenced by a priori assumptions. To minimize this influence, it is recommended that the studies of long-term trends using buv data be restricted to 1–20 mbar range. Outside this range, only the column amounts of ozone between 20 mbar and surface, and above 1 mbar, can be considered relatively free of a priori assumptions.

1. Introduction

In this paper we describe the algorithm used by NASA's Ozone Processing Team (OPT) to obtain ozone profiles from measurements made by the Solar Backscatter Ultraviolet (SBUV) experiment [*Heath et al.*, 1975; *Heath et al.*, 1978] on the Nimbus 7 satellite, and by its follow-on SBUV/2 instruments on NOAA polar satellites. The same algorithm is used to process data from the SSBUV instrument that flies on NASA's Space Shuttle. The SBUV instrument operated from November 1978 until June 1990. Three SBUV/2 instruments have been flown since December 1984, of which two are currently operational. Eight flights of the SSBUV have been made since October 1989 at 9–12 month intervals. Data from all these instruments have now been processed using the algorithm described in this paper and the best current understanding of instrument calibration [*Herman et al.*, 1991; *Weiss et al.*, 1991; *Hilsenrath et al.*, 1993; *Hilsenrath et al.*, 1995; *Bhartia et al.*, 1995]. The combined 16-year record of ozone profiles produced from these instruments is the only global data set of its kind. The SBUV and SSBUV data are archived at NASA's Distributed Active Archive Center (DAAC), Goddard Space Flight Center, Greenbelt, Maryland. SBUV/2 data are archived at NOAA's National Climate Data Center (NCDC), Ashville, Tennessee. In the following we shall use the lower case letters "buv" as a generic abbreviation for "backscattered ultraviolet," and the upper case letters, for example, SBUV, to refer to specific instruments.

The buv measurement series started with the launch of the BUV instrument on the Nimbus 4 satellite in April 1970. An early algorithm [*Mateer et al.*, 1971] was used to process some of the first data from the BUV experiment [*Krueger et al.*, 1973]. This algorithm used the "pressure increment" (PI) atmospheric model formulation of *Yarger* [1970] and the minimum information mathematical inversion procedure of *Twomey* [1963]. The OPT, formed by NASA in 1974, took over the responsibility for calibration, algorithm development, validation, and archival of data from all buv experiments, including those from the total ozone mapping spectrometer (TOMS) instrument that uses a similar technique to produce high-resolution global maps of total column ozone. The OPT continues to have calibration and algorithm responsibility for NOAA's SBUV/2 instrument series. In the intervening years, the OPT has developed several versions of the ozone processing algorithm [*Bhartia et al.*, 1981; *Klenk et al.*, 1983; *Fleig et al.*, 1990]. The algorithm described in this paper is the most recent version (V6.0) of such algorithms, now the operational NASA and NOAA algorithm.

In the following sections, we describe the main features of the buv ozone profile algorithm, starting with a brief description of the instruments, followed by a description of the forward model used in computing the radiances, given the atmospheric parameters. Next, we describe the inverse model used to calculate the ozone vertical profiles from the buv measurements. This includes a discussion of two semi-analytical schemes that provide total column ozone and ozone profiles near 1 mbar (1 mbar = 1 hPa) using measurements at selected buv wavelengths. Using this information, the algorithm estimates the multiple scattering component of the measured radiance and constructs a first-guess profile. In the sections that follow the inverse model discussion, we discuss the information content of the buv measurements and the errors in retrieved profiles.

2. BUV Instruments

All instruments considered in this paper use a double monochromator to measure buv radiances in 12 fixed wavelength bands with 1.1 nm bandwidth. The nominal wavelengths and the actual center wavelength for SBUV are given in Table 1. The follow-on SBUV/2 and SSBUV instruments have similar

[1]Laboratory for Atmospheres, NASA Goddard Space Flight Center, Greenbelt, Maryland.
[2]Scarborough, Ontario.
[3]Software Corporation of America, Lanham, Maryland.
[4]Hughes STX Corporation, Greenbelt, Maryland.

Paper number 96JD01165.
0148-0227/96/96JD-01165$09.00

Table 1. Spectroscopic Parameters for the Nimbus 7/SBUV Instrument

Nominal Wavelengths, nm	Actual SBUV Wavelengths, nm	Rayleigh Scattering Coefficient, $(atm)^{-1}$	Ozone Absorption Coefficient, $(atm\text{-}cm)^{-1}$
255.5	255.7	2.457	309.7
273.5	273.6	1.813	169.9
283.0	283.1	1.566	79.88
287.6	287.7	1.460	48.33
292.2	292.3	1.363	27.82
297.6	297.6	1.261	13.66
301.9	302.0	1.183	7.462
305.8	305.9	1.119	4.281
312.5	312.6	1.020	1.632
317.6	317.6	0.953	0.868
331.2	331.3	0.796	0.140
339.8	339.9	0.713	0.025

Other instruments in the buv series have similar wavelengths except for the shortest wavelength band, which has been moved to 252.2 nm for the newer instruments. The ozone absorption coefficient has been calculated for 1.1-nm instrument band pass at a nominal atmospheric temperature at the location of the peak of the contribution function.

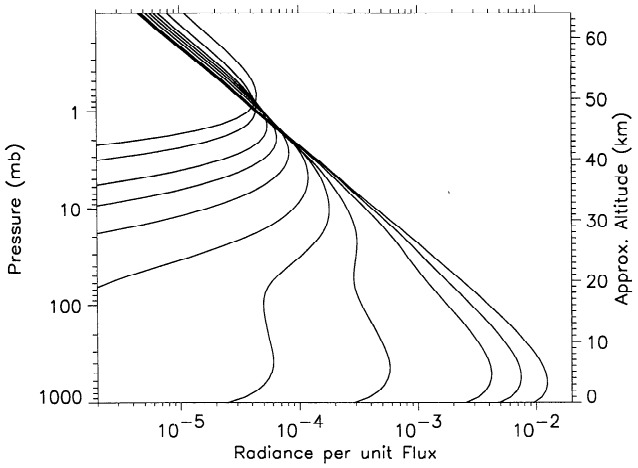

Figure 1. Radiance contribution from ~0.8 km ($\Delta \log p$ = 0.115) atmospheric layers at buv wavelengths at 45° solar zenith angle for a midlatitude 325 DU ozone profile. Computation includes all orders of scattering for surface reflectivity of zero. The shortest wavelength (255.5 nm) peaks at the top, longest (331.2 nm) peaks at the bottom. (339.8 nm wavelength, which is used for determining reflectivity, is not shown.)

wavelengths, except for the shortest-wavelength band which was moved to 252.2 nm to avoid contamination by the NO-γ O4 band [*McPeters*, 1989] emission at 256 nm. (For exact center wavelengths of these instruments, as well as for other instrument-specific information, see their respective user's guide available from the data archive centers. To avoid confusion, we shall use nominal wavelengths to refer to individual buv bands.) The instrument steps through these wavelengths in sequence over 32 s, while viewing the Earth in the fixed nadir direction with an instantaneous field of view (IFOV) on the ground of 183 by 183 km (except for SSBUV which has an IFOV of 50 by 50 km due to the lower orbital altitude of the shuttle). During the 32-s scan time the satellites move approximately 200 km along their tracks, so there is a 17-km gap between the IFOVs at a given wavelength (except for SSBUV, which has 150-km gaps). To account for the change in the scene-reflectivity due to the motion of the satellite during the course of a scan, a separate coaligned filter photometer (centered at 343 nm on SBUV; 380 nm on SBUV/2 and SSBUV) makes 12 measurements concurrent with each of the 12 monochromator measurements.

The buv instruments are designed to measure both the backscattered UV radiation from Earth and the incoming solar flux. Since ozone information is derived from the ratio of these measurements, optical properties of the instrument components common to both measurements cancel out and do not need to be characterized. For solar flux measurements, an aluminum diffuser plate rotates into the instrument's field-of-view to reflect the solar beam into the instrument when the satellite is over the northern terminator. (SSBUV has a transmission diffuser. The shuttle is rotated in an appropriate orientation so the instrument can view the sun.) Since this plate is not used in Earth radiance measurements, accuracy in characterizing its bidirectional reflectivity, both prelaunch and during space operations, is a major factor in determining the accuracy of ozone profiles derived from the buv instruments. Since the SBUV diffuser plate suffered slow continuous degradation in space throughout its lifetime [*Cebula et al.*, 1988], apparently due to the solarization of contaminants deposited on its surface, the SBUV/2 series of instruments were designed with an internal calibration lamp to characterize the reflectivity of the plate as a function of time [*Weiss et al.*, 1991]. Long-term calibration of SBUV has required the development of indirect calibration techniques that rely on the internal consistency of measurements at different wavelength bands to infer calibration drifts [*Herman et al.*, 1991; *Bhartia et al.*, 1995].

Figure 1 illustrates the physical basis of the buv method for estimating the ozone profile. It shows the contribution to the buv radiances from different levels in the atmosphere. With increasing wavelength, the photons penetrate more deeply into the atmosphere, and thus sample different regions of the atmosphere. At wavelengths longer than 310 nm, the buv photons scatter from the lower troposphere. Measurements at these wavelengths provide the total column ozone, which is used as input to the buv profile algorithm. One notes that at the two middle buv wavelengths (301.9 and 305.8 nm), the radiance contribution comes from a very broad region of the atmosphere (0–40 km). These wavelengths are sensitive only to the broad features of the ozone density profile, such as the column amount and the mean (density-weighted) altitude.

3. Forward Model

The problem of estimating buv radiances from Earth's atmosphere varies considerably in complexity depending upon wavelength. At wavelengths shorter than 290 nm, where strong ozone absorption (Figure 1) sharply cuts off the penetration of photons below 30 km, the buv radiances can be calculated by solving a relatively simple single-scattering problem in a purely Rayleigh atmosphere. However, at longer wavelengths the buv photons penetrate deep into the troposphere where they not only suffer multiple scattering in the optically thick Rayleigh atmosphere but are also affected by terrestrial surfaces, aerosols, and clouds. Given the computational complexity of these effects, it is convenient to consider the buv radiances as composed of two parts. The single-scattered (SS) component, that includes just the primary scattering in an atmosphere consisting only of Rayleigh scatterers, and the multiple-scattered

and -reflected (MSR) component, that includes all other types of scattering and surface effects. During operational processing, the SS component is estimated accurately by numerical quadrature. However, the MSR component is estimated separately using a table look-up procedure. We describe the details of the computational procedure below.

3.1. Ozone Absorption and Rayleigh Scattering Coefficients

The Rayleigh scattering cross sections used in the buv forward model are based on the work of *Bates* [1984], and the ozone absorption cross sections are based on the measurements of *Bass and Paur* [1984]. Since the buv instruments measure the average radiance in a 1.1-nm band, while the radiative transfer models provide radiance per unit solar flux at monochromatic wavelengths, one must integrate the product of calculated radiances and the solar spectrum over the instrument band pass to simulate the measured radiance. For computational simplicity, effective absorption and scattering cross sections that yield the same radiance as obtained by integrating the monochromatic radiances are defined for each band of the instrument. Instrument bandpass-weighted average cross sections provide a good initial estimate of effective cross sections. These estimates are adjusted iteratively [*Klenk*, 1980] until they yield nearly the same radiances as obtained from exact calculation for a typical observing condition. The effective cross sections are converted into scattering and absorption coefficients, given in Table 1, by assuming 2.149×10^{25} air molecules/cm^2 in 1 atm column of air [*Penndorf*, 1957] and 2.6868×10^{19} O_3 molecules/cm^2 in 1 atm-cm column of ozone.

3.2. Primary Scattering

Considering only Rayleigh scattering and ozone absorption, the single-scattered component I_{ss} of the buv radiances is given by,

$$I_{ss} = F_\lambda \frac{\beta^*_\lambda P(\Theta)}{4\pi} \int_0^{p_s} \exp\left[-S_x(p)\alpha^*_\lambda X(p) - S_p(p)\beta^*_\lambda p\right] dp \tag{1}$$

Where, F_λ is the solar flux at wavelength λ, β^*_λ is the effective Rayleigh scattering coefficient per unit pressure, $P(\Theta)$ is the Rayleigh scattering phase function for a scattering angle Θ, α^*_λ is the effective ozone absorption coefficient per unit ozone amount, $S_x(p)$ is the slant path (air mass) through ozone of the radiation scattered from pressure p, $S_p(p)$ is the slant path through air, $X(p)$ is the column ozone above the pressure p, and p_s is the surface pressure.

For a nadir-viewing instrument at solar zenith angle θ_0, $\Theta = \pi - \theta_0$, and,

$$P(\Theta) = \frac{3}{2}\frac{1+\rho}{2+\rho}\left(1 + \frac{1-\rho}{1+\rho}\cos^2\theta_0\right) \tag{2}$$

where, ρ is the molecular anisotropy factor, calculated from King's factor F_k given by *Bates* [1984] using, $\rho = 6(F_k - 1)/[10 + 7(F_k - 1)]$.

For a nadir-viewing instrument, in the plane parallel approximation, $S_x(p) = S_p(p) = 1 + \sec\theta_0$. However, when the Earth's sphericity is considered,

$$S_x(p) = 1 + \frac{1}{X(p)} \int_0^{z(p)} \sec\left[\theta(z')\right] \frac{dX(z')}{dz'} dz', \tag{3a}$$

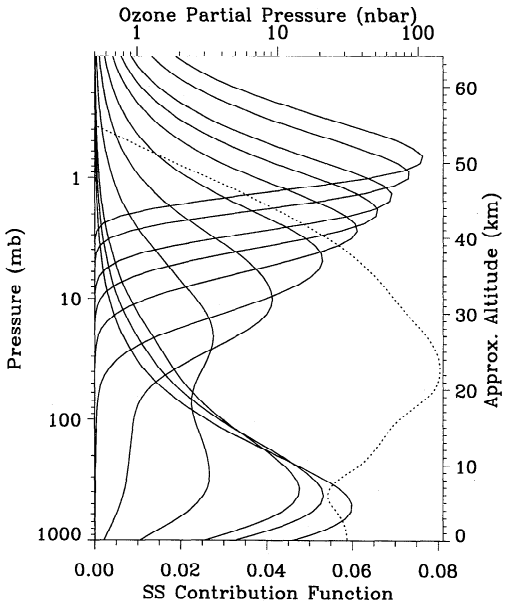

Figure 2. Single-scattering contribution function, normalized to total radiance, that is, $(\delta \log I_{ss}/\delta \log p)(I_{ss}/I)$, for the Figure 1 observing conditions. The shortest wavelength (255.5 nm) peaks at the top, longest (331.2 nm) peaks at the bottom. Dashed line shows the ozone profile.

and,

$$S_p(p) = 1 + \frac{1}{p} \int_0^{z(p)} \sec\left[\theta(z')\right] \frac{dp(z')}{dz'} dz' \tag{3b}$$

where $z(p)$ is the altitude at the pressure p, and $\theta(z')$ the solar zenith angle at altitude $z(p')$ of the ray scattered from $z(p)$, is given by,

$$\theta(z') = \mathrm{Sin}^{-1}\left[\frac{R + z(p)}{R + z(p')} \mathrm{Sin}\ \theta_0\right], \tag{4}$$

where R is the radius of the Earth. Since ozone absorption coefficients and $z(p)$ are functions of atmospheric temperature, computation of I_{ss} using (1) requires the knowledge of the atmospheric temperature profile. In most cases, a standard atmospheric temperature profile provides adequate accuracy.

If one divides the atmosphere in layers of equal $\Delta \log p$, the fractional contribution to the radiance from each layer is defined by the contribution function, $C(p)$. From (1), in the plane-parallel approximation ($S = S_x = S_p$),

$$C_\lambda(p) = pe^{-S(\alpha^*_\lambda X + \beta^*_\lambda p)}. \tag{5}$$

Figure 2 shows the plot of $C(p)$ for a typical observing condition. By differentiating $C(p)$ with respect to $\log p$, we find that the peak of the contribution function forms at a pressure p_k, where,

$$\alpha^* S \left.\frac{\partial X}{\partial \log p}\right|_{p_k} + \beta^* S p_k = 1. \tag{6}$$

At shorter buv wavelengths, the first term is much larger than the second, so the peak forms in the atmosphere where $\partial X/\partial \log p \approx 1/\alpha^* S$. (Note that $\partial X/\partial \log p$ defines the partial pressure of ozone, which is customarily given in nanobars. To get nanobars, divide α^*, given in Table 1, by 1266.) Since the

peak position varies with αS, one can scan the atmosphere either by varying α or S. The buv technique uses the former method; the ground-based Umkehr technique, which is based on similar principles, uses the latter method. The longest 4 buv wavelengths usually get their maximum contribution from the troposphere, where the first term becomes much smaller than the second, so the peak forms at $p_k = 1/\beta^* S$ atm (for β^* in atm^{-1}). These wavelengths are sensitive to the column ozone above p_k as well as to the ozone distribution near p_k. However, given the small ozone density in the troposphere, the latter effect is small. At intermediate wavelengths, two separate peaks can form from each of the two terms in (6). These wavelengths are sensitive to total column ozone as well as to the stratospheric ozone profile. The peak position and hence the information content of the radiances at any given wavelength, changes with solar zenith angle. Thus a wavelength suitable for determining total ozone at small solar zenith angle may become too sensitive to ozone profile to be used for that purpose at large solar zenith angle. For wavelengths for which the first term in (6) is significant, the peak position also depends on the ozone profile itself. Thus, given an ozone profile and measurement solar zenith angle, equation (6) provides a quick method of assessing the information content of the buv radiances at a particular wavelength.

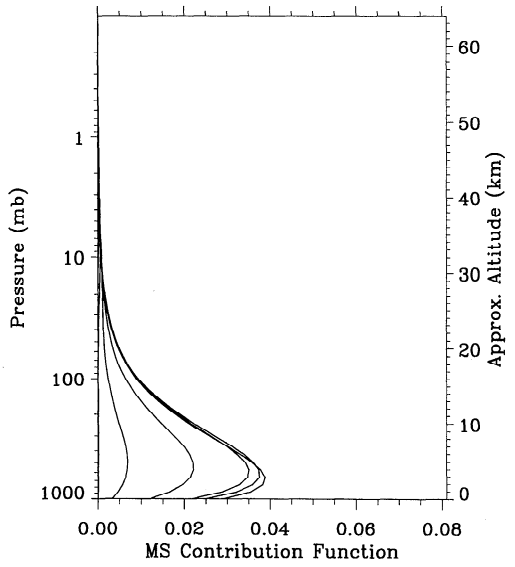

Figure 3. Multiple scattering contribution function, normalized to total radiance, that is, $(\delta \log I_{ms}/\delta \log p)(I_{ms}/I)$, for longest 5 buv wavelength (297.6 nm–331.2 nm) where MSR is nonzero (339.8 nm wavelength not shown). (Shorter wavelengths have smaller peaks.)

3.3. Multiple Scattering and Reflection

At wavelengths longer than 290 nm, the incoming photons penetrate into the lower atmosphere where they may undergo multiple scattering. In addition, one must consider the effects of surface reflection and Mie scattering by aerosols and clouds. Since these effects are highly variable and cannot be modeled accurately, the buv technique relies on the concept of Lambert-equivalent reflectivity, introduced by *Dave* [1977]. In this concept, one estimates the buv radiances by radiative transfer calculation for an idealized atmosphere that contains ozone and Rayleigh scatterers, but no Mie scatterers, and is bounded by an opaque Lambertian surface. The effective reflectivity, R^*, and effective pressure, p^*, of this fictitious surface are estimated by using the measured radiance at the longest buv wavelength (339.8 nm), where the ozone absorption is very weak. Since scattering by clouds and aerosols is not explicitly considered in the model, and the surfaces are considered Lambertian, *Dave* [1977] called the R^* so derived the Lambert-equivalent reflectivity (LER). Although the implementation details are different, the concept of LER is similar to the concept of "window channel" used in infrared remote sensing, where R^* becomes the effective surface emissivity. As in the infrared, for the concept to work, one must assume that the wavelength dependence of R^* is negligible so that the same value of R^* can be used to estimate the radiances at the shorter, ozone-absorbing wavelengths.

Closely related to the concept of R^* is the concept of p^*, which is the pressure at which the contribution to the buv radiances effectively cuts off. The p^* determines the column amount of air, hence the number of buv photons generated by Rayleigh scattering. It also determines the amount of ozone seen by the photons, hence the total amount of absorption. The first effect is most important at low reflectivities where p^* can be estimated accurately using terrain height tables. At higher reflectivities, p^* is estimated using an empirical algorithm that accounts for clouds and snow/ice [*Fleig et al.*, 1990]. Fortunately, at high reflectivities, when the estimation of p^* is most uncertain, MSR depends primarily on the column amount of ozone above p^*, which can be estimated accurately using the longer wavelength radiances, as discussed later.

The MSR radiances are computed by using the auxiliary equation solutions of the radiative transfer equation [*Dave*, 1964], which accounts for polarization and all orders of scattering. However, Earth's sphericity effects are included only in the calculation of primary scattering, using (3). Higher-order scattering is assumed to take place in a plane-parallel atmosphere. Recent calculations [*Caudill*, 1994] indicate that this approximation produces errors of less than 1% in radiances at solar zenith angles up to 88°.

Using Dave's notation, the buv radiance for a Lambertian surface of reflectivity R^* can be written as,

$$I = I_0 + \frac{R^* T}{1 - R^* S_b}, \tag{7}$$

where, I_0, T, and S_b are each functions of α^*, β^*, p^*, θ_0, $X(p)$, and $T(p)$. For computational efficiency, a table look-up procedure is used to compute the MSR component of I. A table of I_0, T, and S_b are precomputed for 10 values of θ_0, 2 values of surface pressure, and 23 standard ozone profiles $X(p)$. The profiles contain different amounts of total column ozone and are divided into 3 sets (3 for low latitude, 10 each for middle and high latitudes). Different climatological temperature profiles are used with each set of ozone profiles. Given a value of R^* and p^* from the 339.8 nm measurements, I is computed using (7), from which I_{ss} is subtracted to get I_{msr}.

The table look-up procedure works because the ozone profile dependence of I_{msr} is weak. As seen in Figure 3, the MSR radiation is generated primarily in the troposphere and is thus controlled by the direct and diffuse radiation reaching the troposphere. At small solar zenith angles, the diffuse component of the radiation reaching the troposphere is relatively small, therefore, I_{msr} depends primarily on total column ozone amount Ω, and closely follows the Beer's law absorption curve,

that is, $I_{msr} \propto \exp(-\alpha^* S\Omega)$. However, at large solar zenith angles, when most of the radiation reaching the troposphere is the diffuse radiation emanating from the middle stratosphere, I_{msr} becomes nearly proportional to I_{ss}. The following procedure is designed to handle both these extremes.

It is assumed that, in general, $I_{msr} = a(\theta_0, \Omega) + b(\theta_0, \Omega) I_{ss}$, where both a and b depend on the total ozone Ω but not on the ozone profile. Since $I = I_{ss} + I_{msr}$, one can write $I_{msr} = a' + b'I$, where a' and b' are also functions of just the total ozone. Thus, given the measured radiances I_{meas}, one can estimate its I_{msr} component by linear interpolation among a set of tabulated values of I and I_{msr}. Given I and I_{msr} for the 23 standard ozone profiles, I_{msr} corresponding to I_{meas} can be written as follows,

$$I_{msr} = I_{msr}(\chi_1) + [I_{msr}(\chi_2) - I_{msr}(\chi_1)] \frac{[I_{meas} - I(\chi_1)]}{[I(\chi_2) - I(\chi_1)]} \qquad (8)$$

where, χ_1 and χ_2 are two standard profiles that contain the same total ozone amount as the measured total ozone, but have different vertical structures to yield significantly different values of I.

4. Inverse Model

The general problem of inverting buv measurements to derive an ozone profile is ill-conditioned. One must apply some sort of constraint to achieve a physically reasonable solution. There are several ways of specifying these constraints. One may, for example, constrain the profile to follow a predefined mathematical function with adjustable parameters that are selected to best fit the measurements; or select a profile that has the highest probability of being the correct profile [*Rodgers*, 1976] based on a priori statistical information. The buv profiling algorithm uses a combination of both of these strategies.

The ozone profile is mathematically defined by a cubic interpolating spline (in the $\log X$ versus $\log p$ coordinate system) with 12 fixed nodes at $p = 2^{-n}$ atm (1 atm = 1013.25 hPa), where $n = 0, 2, 3 \ldots 12$ (note that $n = 1$ is missing). The algorithm first obtains X at $n = 0$, that is, the total column ozone, using the longest 4 buv wavelengths. Total ozone is used to estimate I_{msr} as well as to select first-guess ozone values at the lowest 5 nodes from a library of ozone profiles. Next, ozone values at the 4 uppermost nodes are estimated using measurements at the shorter buv wavelengths. A cubic spline curve fitted to these 9 nodes forms the starting profile, which is iteratively adjusted until the retrieval converges to a solution profile. The following subsections discuss this procedure in more detail.

4.1. Retrieval of Total Column Ozone

Total ozone is derived using the 4 longest wavelength bands of the instrument [*Dave and Mateer*, 1967; *Mateer et al.*, 1971; *Klenk et al.*, 1982; *McPeters et al.*, 1993]. Since these references discuss the total ozone algorithm in adequate detail, we provide here just an overview.

The buv total ozone technique is based on the observation made earlier that at certain wavelengths the buv photons penetrate most of the ozone column to reach the troposphere, whence they are scattered by the dense atmosphere, clouds, aerosols, and surface. When the peak of the contribution function is in the troposphere, the logarithms of buv radiances decrease almost linearly with ozone column amount, approximately following the Beer's law of absorption. Since this relationship is not perfectly linear but has a small dependence on ozone profile and temperature, one needs to perform accurate radiative transfer calculations using climatological profiles to describe the curves relating the buv radiances to total column ozone under a variety of observing conditions. This procedure was described in section 3.3. To reduce errors due to possible spectral dependence of R^*, the algorithm obtains total ozone using a pair of wavelengths that are chosen to be less than 20 nm apart.

4.2. Retrieval of Ozone Profile Near 1 mbar

For the shorter buv wavelengths $\alpha^* SX(p) \gg \beta^* Sp$, so the integral in the single scattering radiative transfer (1) has the form of the Laplace transform of the ozone profile $X(p)$. It has an analytical solution if the ratio of ozone to atmospheric scale height (σ) can be assumed to be constant in the range of pressures where the value of the integrand is significant. The latter assumption implies that the cumulative ozone X above a pressure p varies as $X = X_0(p/p_0)^{1/\sigma}$, where X_0 is the ozone column above a reference pressure p_0. With these assumptions, one can write the solution of (1) as,

$$Q_\lambda = p_0(\alpha^*_\lambda S X_0)^{-\sigma} \Gamma(1 + \sigma), \qquad (9)$$

where Q, which has the dimension of pressure, is related to the ratio of Earth radiance (I) to the incoming solar flux (F) by $Q = 4\pi/\beta^* P(\theta_0)\ I/F$. The slant path S can be calculated accurately using the Chapman function $Ch(\theta)$ [*Fitzmaurice*, 1964], by $S = 1 + Ch(\theta)$, using the product of σ and atmospheric scale height as the ozone scale height.

Using (9) one can solve for both X_0 and σ from buv measurements made at just 2 wavelengths. If additional wavelengths are available, then one may improve the estimates of X_0 and σ by using least square regression to solve (9), provided σ can be assumed to be constant in the range of altitudes sampled by the wavelengths. This is generally true for shorter buv wavelengths whose contribution functions (Figure 2) peak above 2 mbar ($\lambda < 290$ nm). This technique for inverting buv measurements has a long history [*McPeters*, 1980]. It was first used for the evaluation of single channel buv measurements from a U.S. Air Force satellite [*Rawcliffe and Elliott*, 1966].

From (9), the quantity Q, and hence the buv albedo from which it is obtained, has a direct physical meaning: $Q/\Gamma(1 + \sigma)$ is the pressure p_0 at which the absorption optical path of the buv radiation through the ozone column above p_0, $\alpha^* SX_0$, becomes unity. *Thomas and Holland* [1977] (TH) first made the observation that for typical values of σ in the upper stratosphere (0.4–0.7), $\Gamma(1 + \sigma)$ is almost a constant, with a value very close to 0.90. Therefore, the buv measured Q at any given wavelength directly provides the value of column ozone, $X_0 = 1/\alpha^* S$, above the pressure $p_0 \approx Q/0.90$.

On the basis of this observation, R. W. L. Thomas and A. C. Holland (personal communication, 1983) suggested that by relating ozone column amounts to pressures derived from Q values at multiple buv wavelengths, it may be possible to retrieve a profile that is nonlinear in $\log X$-$\log p$. Although their proposed method is used in the current algorithm, simulation results show that the improvement resulting from the TH modifications are modest. In most cases, the method does no better than the simple 2-parameter (X_0, σ) retrieval method discussed before.

4.3. Construction of First-Guess Profile

The first-guess profile is constructed by fitting a cubic interpolating spline with natural boundary conditions to the log X versus log p curve. The piecewise linear curve given by the TH solution, linearly extrapolated, provides the cumulative ozone X at the 4 topmost points, at $p = 2^{-n}$ atm, with $n = 9, 10, 11, 12$. The value of X at $n = 0$ is simply the total column ozone. Values of X at $n = 2, 3, 4, 5$, are obtained using a library of standard ozone profiles. This library was constructed by combining data from the Stratospheric Gas and Aerosol Experiment (SAGE) [*McCormick et al.*, 1989] with ozonesonde data, and contains 46 profiles, 23 in each hemisphere. Each group of 23 profiles is further subdivided into 3 sets representing low (15°), middle (45°) and high (75°) latitudes. There are 10 middle and high-latitude profiles for total ozone ranging from 125 DU to 575 DU in 50 DU steps, and 3 low-latitude profiles for 225, 275, and 325 DU total ozone. A profile for a given total ozone amount and latitude of measurement is obtained by bilinear interpolation (low-latitude profiles are extended to the equator and high-latitude profiles to the pole). Given the values of X at the 9 nodes, the values at the missing 3 nodes ($n = 6, 7, 8$) are obtained by spline interpolation.

4.4. Retrieval of Final Ozone Profile

The buv algorithm assumes that the MSR component of the total measured radiation contains no retrievable ozone profile information. Since the total ozone information that it does contain has been obtained previously using the longer buv wavelengths, I_{msr} is treated simply as a contamination to the measured radiance and is subtracted out using the estimation procedure described in section 3.3. The retrieval scheme, therefore, is based on single-scattering kernels and single-scattered radiances. In addition, measurements made at the longest 4 wavelengths (3 at high solar zenith angles) that have already been used in deriving R^* and Ω are not used explicitly. Instead, the total ozone Ω derived from them is considered a measurement and is included with the radiance measurements at the other 8 wavelengths (9 at high solar zenith angles, by including the 312.5 nm wavelength). (For reasons discussed earlier, Nimbus 7/SBUV algorithm does not use the shortest wavelength.)

Although this scheme of handling the measured radiances may appear unnecessarily tedious, it was done primarily to save computation time. Back-calculations using the retrieved profiles show that, in most cases, the derived ozone profile explains the measured radiances at all 12 wavelengths to a high degree of precision (~1%).

The final retrieval of ozone profile is a straightforward implementation of equation (101) of *Rodgers* [1976] reproduced below.

$$x_{n+1} = x_0 + S_x K_n^T (K_n S_x K_n^T + S_\varepsilon)^{-1}[(y - y_n) - K_n(x_0 - x_n)] \quad (10)$$

In this equation, x_0 is the a priori profile. The solution starts with a first-guess profile x_1, from which the kernels K_1 and measurements y_1 are evaluated, and proceeds through n iterations until the retrieved profiles stop changing to within a specified tolerance. Although x_1 is not required to be the same as x_0, they are made the same in the buv algorithm. Strictly speaking, since measured radiances are used in constructing x_0, one does not have a true a priori profile to which the solution is constrained. According to C. D. Rodgers (private communication, 1992), this violates the tenets of optimal estimation theory upon which (10) is based. However, the principal impact of this violation is to complicate the error analysis of the algorithm. We will discuss this issue in the next section.

Table 2. Definition of Atmospheric Layers Used by the Algorithm

Layer Number	Pressure Range, mbar	Pressure at Layer Center, mbar	Approx. Altitude at Layer Center, km
1	253–1013	507	5.5
2	127–253	179	12.5
3	63.3–127	89.6	17.0
4	31.7–63.3	44.8	21.3
5	15.8–31.7	22.4	25.8
6	7.92–15.8	11.2	30.4
7	3.96–7.92	5.60	35.2
8	1.98–3.96	2.80	40.2
9	0.99–1.98	1.40	45.4
10	0.495–0.990	0.700	51.0
11	0.247–0.495	0.350	56.5
12	0.0–0.2467	–	–

They are similar to those used by the ground-based Umkehr technique.

In applying (10) to the buv inversion problem, the measurement vector y has 9 elements: 8 values of log Q (with Q as defined in section 4.2) and total ozone Ω. (Dimensions increase by one at high solar zenith angles, and reduce by one for SBUV.) The vector x, representing the unknown profile, has 12 elements: logω, where ω, the layer ozone amount is defined as, $\omega_i = X_i - X_{i+1}$, for $i = 1, 2, 3 \ldots 11$; $\omega_{12} = X_{12}$. (Traditionally, buv algorithms have used logω, rather than ω as unknowns, to avoid the possibility of getting negative layer ozone. Unfortunately, this makes the kernels $K = \delta\log Q/\delta\log\omega$ highly nonlinear at longer wavelengths and slows down convergence. This is one of the reasons why measured total ozone is used to select a good first-guess profile in the lower stratosphere.) Note that the buv layers are similar to those used by the ground-based Umkehr technique [*Mateer and DeLuisi*, 1992]. Table 2 provides the pressure and nominal altitude of these layers.

Using the above definition of measurements y and unknowns x, the a priori covariance matrix S_x and the measurement error covariance matrix, S_ε, can be defined. S_x is constructed using the information given in Table 3. These were obtained using ozonesonde profiles for layers 1 through 5, and

Table 3. Information Used in Constructing the A Priori Covariance Matrix S_x

Layer Number	Layer std. dev, percent	L, L + 1 correlation	L, L + 2 correlation
1	25.0	0.0	−0.55
2	35.0	0.0	−0.55
3	25.0	0.45	−0.55
4	15.0	0.45	−0.55
5	10.0	0.45	0.0
6	10.0	0.55	0.0
7	8.0	0.61	0.0
8	8.0	0.56	0.0
9	8.0	0.0	0.0
10	8.0	0.0	0.0
11	10.0	0.0	
12	12.0	–	

Table 4. These Values May be Used to Assign 1σ "Error Bars" to Single BUV Profiles

Pressure, mbar	Ozone Mixing Ratio Error, Percent
0.3	10
0.4	7
0.5	6
0.7	6
1.0	6
1.5	6
2.0	5
3.0	5
4.0	5
5.0	5
7.0	5
10	5
15	6
20	7
30	9
40	11
50	12
70	13
100	15

They are obtained by examining the errors in retrieving simulated 5 km resolution ozone profiles constructed from SAGE II dataset. Note that the errors have large systematic component, so they do not necessarily reduce when profiles are averaged.

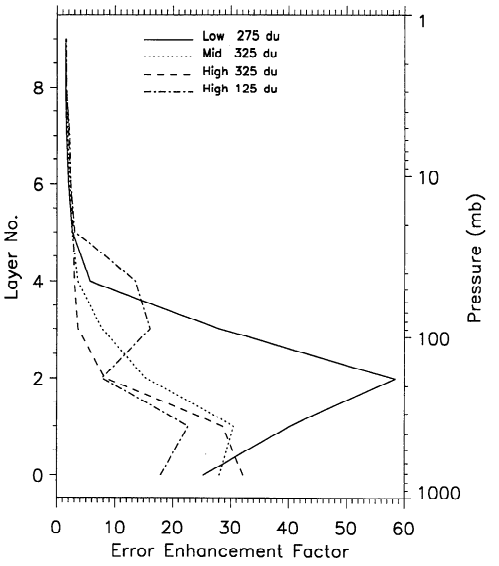

Figure 4. Error enhancement in computing layer ozone amounts for ~5 km Umkehr layers by numerical differentiation of cumulative ozone profiles with fixed random errors at all altitudes.

using buv ozone profiles for layers 6 and above, from a previous version (Version 4) of the algorithm. However, simulation results show that details of the S_x matrix are relatively unimportant, for the algorithm incorporates most of the a priori information in constructing the first-guess profile. Indeed, a simple diagonal S_x matrix would have done just as well.

In constructing the matrix S_ε, one needs to account for the errors in the MSR-corrected measurements, rather than the measurements themselves. The MSR correction produces two effects. First, the measurement noise (assumed to be 0.5% at all wavelengths) gets scaled up by the ratio I/I_{ss}, and second, uncertainty in the MSR correction adds additional noise at those wavelengths where the correction is significant. Simulation results show that uncertainty in total ozone produces the largest uncertainty in I_{msr}, and since this uncertainty is correlated between wavelengths, the S_ε matrix becomes nondiagonal. However, like S_x, the S_ε matrix also plays a minor role in the inversion. For additional details about constructing the two covariance matrices, and other implementation details, the readers are referred to the appropriate references [*Klenk et al.*, 1983; *Fleig et al.*, 1990].

4.5. Reporting of Profiles

Ozone profiles derived from the inversion are reported as 12 layer ozone amounts (in Dobson units) defined above, as well as ozone mixing ratios at 19 standard pressure levels, given in Table 4. The latter are obtained from the first derivative of the cubic spline curve. However, as discussed in previous sections, the buv radiances are directly sensitive to the column amount of ozone above a pressure surface. To compute layer ozone amounts or mixing ratios, one must difference two numbers. In the upper stratosphere, where the column amount of ozone is changing rapidly, the numerical differentiation process increases the error only modestly. Below the ozone density peak, however, one must difference two large numbers to obtain a small number. This can lead to large error enhancement, particularly in the tropical lower stratosphere, where the amount of ozone in a layer, as a fraction of the ozone column above, is the smallest. Since many ozone-measuring instruments share this problem, it is instructive to examine these errors.

If X_1 and X_2 are the column amounts of ozone above the pressure p_1 and p_2, respectively, measured with a precision σ and error correlation r, then the fractional error Σ in estimating ozone in the layer p_1-p_2 is enhanced by a factor f, given by

$$f = \sum/\sigma = \frac{\sqrt{(X_1^2 + X_2^2 - 2rX_1X_2)}}{X_1 - X_2} \tag{11}$$

Figure 4 shows that in the lower stratosphere the error enhancement factor for random noise can reach 60 for roughly 5-km-thick Umkehr layers. Since the error is inversely proportional to layer thickness, fractional errors in obtaining lower stratospheric mixing ratios in 1-km layers can be enhanced by more than 2 orders of magnitude. These large errors are often not noticed since the fractional variability of ozone is also very large in the lower stratosphere.

We also note that the common practice of drawing buv (or Umkehr) ozone profiles as a piecewise linear curve joining the layer ozone amounts is misleading. This piecewise curve would not yield the correct radiances, and therefore, does not represent the solution profile. This confusion arises from an often misunderstood feature of inversion methods. For accurate quadrature, one must define the profile at a much higher vertical resolution than what the technique is capable of providing. One can do this either by retrieving the profiles in layers much finer than the inherent resolution of the technique and then joining them by a piecewise linear curve to construct the profile, or by using an appropriate mathematical function, such as the cubic spline, to interpolate between points provided by a coarser resolution retrieval. In either case, the solution profile is the continuous curve upon which one does forward model calculations to show that it can reproduce the measurements to within a specified error.

5. Information Content

In discussing the information content of buv type measurements, *Mateer* [1971] notes that in such problems one faces two types of loss in information about the vertical structure of the observed profile. First, the measurement process itself causes loss of information. This can be seen from Figure 1. Since the radiation at each wavelength comes from a broad range of altitudes, measurements contain little information about small vertical-scale variations in ozone, and such signals may not be observable above the background noise. Although, in principle, one may be able to reduce the background noise by signal processing, and thus observe radiance changes resulting from small-scale variations, there is no unique way of identifying which among the many possible variations in ozone is producing the observed variation in radiance. Therefore, unless one has good a priori knowledge to select one type of variation over another, information in the radiances about small-scale variations cannot be retrieved. This results in an additional loss of information, one that occurs during the inversion process. We consider both types of information loss and their implication for buv ozone measurement.

5.1. Information Content of Measurements

Although there are formal ways of analyzing the information content [*Mateer*, 1971; *Rodgers*, 1976; *Rodgers*, 1990] by using Eigen value analysis to compute independent pieces of information contained in the measurement, much can be learned by examining a plot of the Jacobian, that is, the matrix of partial derivatives that relate change in radiance to changes in ozone profile.

For the buv problem there are at least three ways of constructing the Jacobian. Since they provide complementary views of the information content, we will examine all three. The first of these Jacobians is the contribution function (Figure 2), $\delta \log I/\delta \log p$, which we have already examined in detail. It provides a convenient way of deciding which wavelengths are suitable for total ozone and which have profile information. It also shows why the middle buv wavelengths are most sensitive to stratospheric aerosols [*Torres and Bhartia*, 1995] that reach the altitude where these wavelengths have peak contribution. The pressure-increment method [*Yarger*, 1970] uses this Jacobian as the kernel for the profile inversion.

A second way of defining the Jacobian is by the fractional change in radiances to fractional change in layer ozone amount, that is, $\delta \log I/\delta \log \omega$, where ω is the ozone amount in a fine vertical layer. The current algorithm (section 4.4) uses the single-scattering component of this Jacobian, averaged down to 12 Umkehr layers, to construct the matrix K in (10). From the plot of the Jacobian (Figure 5) one notes that the full-width at half-maximum (FWHM) of the curves that peak in upper stratosphere is 8 km, increasing to 12 km for the lower curves. This limits the vertical resolution achievable from the buv technique. One also notes that the curves are separated by less than one half of their FWHM, indicating that additional wavelengths would not add information. These curves, however, do not depict the information content of the longer buv wavelengths well. For example, it is hard to discern from these curves the information contained in the longer wavelengths about total column ozone and lower stratospheric profile.

The third form of the Jacobian can be defined by fractional change in radiances due to absolute change in a layer ozone amount, that is, $\delta \log I/\delta\omega$. This form is most suitable for understanding the information content of the longer wavelengths. Noting that a total ozone wavelength should have a constant, altitude-independent value of $\delta \log I/\delta\omega$, Figure 6 shows that the 2 buv wavelengths used for total ozone estimation, centered at 312.5 and 317.5 nm, do not have an ideal sensitivity curve. Even in clear sky conditions, assumed for Figure 6, their sensitivities drop significantly in the lower troposphere, a result of large Rayleigh optical thickness. Clouds can reduce the sensitivity even further, and an increase in the

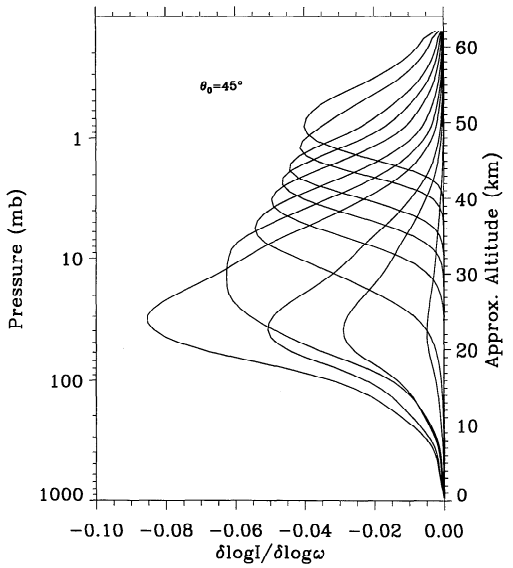

Figure 5. Sensitivity of buv radiances to fractional change in ozone ($\delta \log I/\delta \log \omega$) for Figure 1 observing conditions. Shortest wavelength is at the top. Longest wavelengths overlap at 20 km with sensitivity decreasing with ozone cross section (339.8 nm wavelength not shown). X axis gives percentage change in intensity for 1% change in ozone in ~0.8 km ($\Delta \log p = 0.115$) layers.

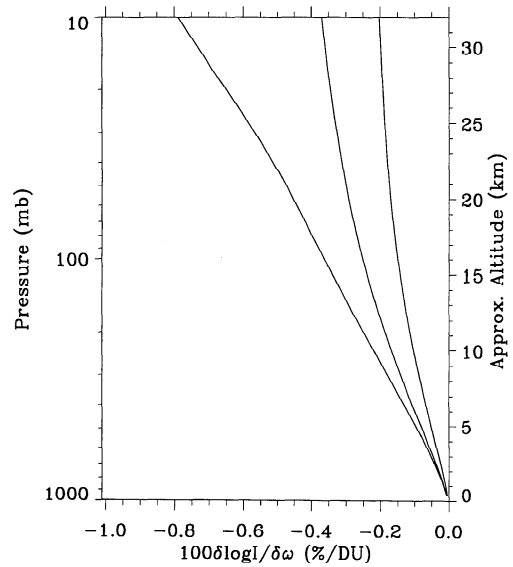

Figure 6. Percentage change in buv radiances due to 1 DU change in ozone ($\delta \log I/\delta\omega$) for Figure 1 observing conditions. Three buv wavelengths (305.8, 312.5, 317.5 nm) are shown that contain most of the information about lower stratospheric ozone. (Shortest wavelength has the greatest ozone sensitivity.)

solar zenith angle raises the altitude where the sensitivity starts to drop. (The drop in sensitivity coincides with the peak in the contribution function, which occurs at $\beta^* Sp_k = 1$, according to (6)). This loss in sensitivity is an important source of error in determining total column ozone from the buv technique [*Klenk et al.*, 1982; *Hudson et al.*, 1995]. From Figure 6, one also notes that 305.8 nm wavelength radiances do contain some information about ozone distribution in the lower atmosphere. Given a change in total column ozone (say from 312.5 nm radiance or from ground-based measurements), 305.8 nm radiance can locate the altitude of the change. The accuracy with which it can do so depends on the signal-to-noise. For example, to detect 1 DU change to within 5 km in altitude one needs 0.1% measurement precision, which may be achievable by signal averaging. However, at best, one has a single piece of information. If the changes occur at multiple altitudes, one can only locate the centroid of the change.

5.2. Information Loss During Inversion

A convenient way of examining loss of information due to inversion is to treat the algorithm as a "black box" and study its response to perturbations in the ozone profile. *Rodgers* [1990] recommends a variant of this technique based on a concept called the averaging kernels (AK). Besides having an elegant physical interpretation, AKs are very convenient for comparing profiles from a low-resolution instrument with those from a high-resolution instrument. Using the AKs and the a priori profile one can immediately tell what profile the algorithm would produce for a given "truth" profile from another sensor. Unfortunately, the AKs cannot be conveniently defined for the current buv profiling algorithm since the algorithm does not use measurement-invariant a priori profile.

Figure 7 shows the response of the algorithm to 8 km Gaussian impulses at different altitudes. Between 1.5 and 20 mbar, the algorithm reproduces the impulse reasonably well except for broadening the FWHM to about 10 km. (These results are derived using the 252 nm wavelength of SBUV/2. If the shortest SBUV wavelength is not used, the upper range of validity drops down to 1.5 mbar at low solar zenith angles, but moves upward as the solar zenith angle increases, in proportion to S $^{\sigma}$, from (9)). At higher or lower altitudes, the response has the wrong shape, with misplaced peak positions. These results are in general agreement with previous conclusions [*WMO*, 1988; *Rodgers*, 1990]. The primary reason for the distorted response is that in the region of the atmosphere where the information from the buv radiances is low, the algorithm relies on a priori information more heavily. Since the Gaussian impulse puts perturbations in the atmosphere that are very different from a priori information, the algorithm finds a compromise answer that poorly reproduces the impulse.

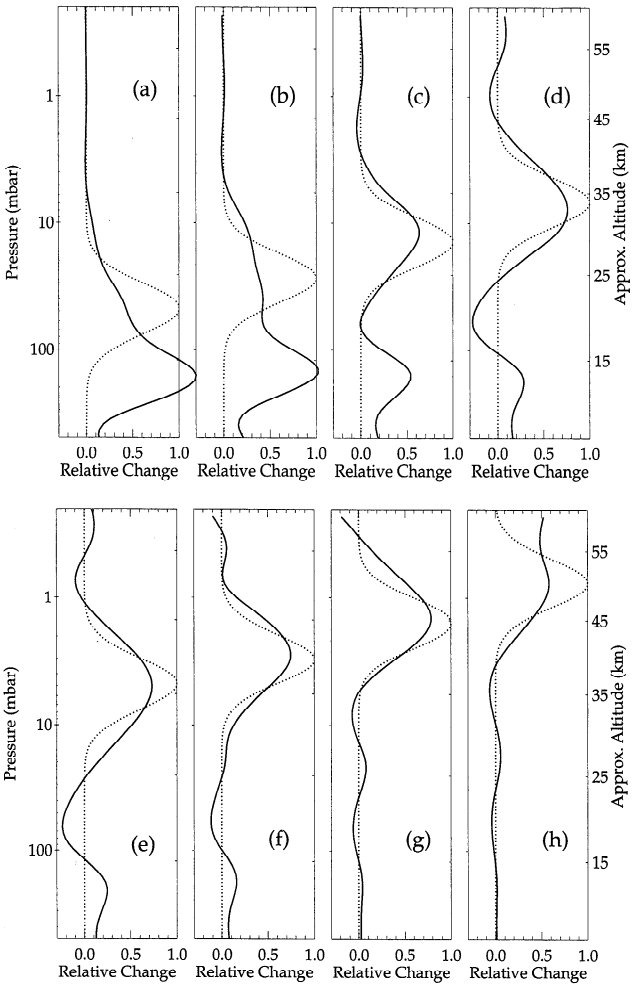

Figure 7. Response of the algorithm to 8-km-wide Gaussian impulse (applied to the logarithm of ozone in roughly 0.7-km layers) at different altitudes. Dashed lines represent the impulse, solid lines represent the response. The algorithm produces broader responses with reasonably located peak positions between 1 and 20 mbar only.

6. Error Analysis

Errors in retrieved ozone profiles come from three independent sources: measurement errors, error in calculating radiances from a known ozone profile, called the "forward model errors", and error in inverting the radiances to obtain an ozone profile, called the "inverse model errors". To estimate these errors, we use high vertical resolution ozone profiles generated by the SAGE instrument.

The SAGE profiles used for this study consist of the SAGE II/SBUV matchup data set created by *McPeters et al.* [1994]. This data set consists of daily mean ozone profiles derived from SAGE II sunrise measurements for the period October 1984 through June 1990. Since SAGE is a solar occultation instrument, these profiles represent the mean of roughly 15 profiles taken at nearly the same latitude but at different longitudes where the satellite saw sunrises during the day. High-resolution SAGE profiles were converted into Umkehr layer ozone values using the pressure versus altitude relationship given on the SAGE data tapes. SAGE usually does not measure the ozone profile in the troposphere, so layer 1 ozone values are not available, and layer 2 values are often unreliable. Since a complete ozone profile is required for this study, layer 1 and 2 ozone values were estimated from layer 3 ozone values using latitude and total ozone dependent climatological profiles (discussed in section 3.3.), to which normally distributed random noise with 25% standard deviation was added. Additionally, the column ozone in layer 12, that is, above 0.247 mbar, was estimated by extending SAGE ozone values in layers 10 and 11 to infinity by assuming a linear $\log X$-$\log p$ relationship, to which 15% random noise was added.

From this data set, consisting of 1655 individual ozone profiles, the buv radiances were computed using the average solar

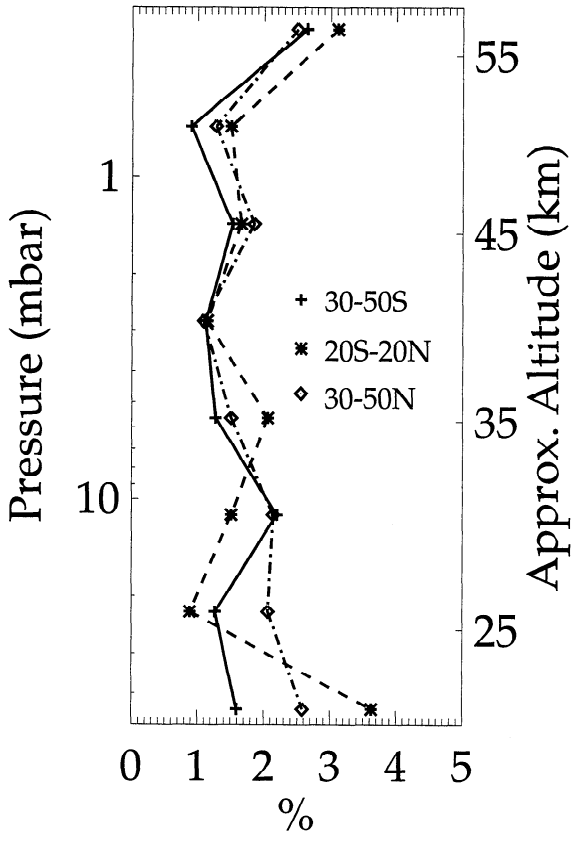

Figure 8. Change in RMS error due to the addition of 0.5% noise at all wavelengths.

zenith angle seen by the SBUV instrument in the latitude band where SAGE took measurements. (Since SBUV is in a sun-synchronous orbit, the solar zenith angles are nearly the same during a day at all SAGE sunrise longitudes, but vary with the season and latitude of measurements.) The computed buv radiances were then used to derive ozone profiles using the algorithm discussed in this paper. Difference between the "true" profiles and the derived profiles are used to estimate the errors discussed below.

6.1. Measurement Errors

Figure 8 shows the effect of 0.5% random noise added to the buv radiances on the SAGE II/SBUV comparison. Not only are these errors small, but given that they are random, they are usually of no consequence, for they average out in a typical application of the buv data. Most important errors, therefore, are systematic errors in calibration.

Experience with both ground and in-orbit calibration of buv sensors flown so far indicates [*Hilsenrath et al.*, 1995] that the largest calibration uncertainty consists of a simple percentage error independent of wavelength. This error comes from uncertainties in determining the bidirectional reflectivity distribution function (BRDF) of the aluminum diffuser carried by these instruments to measure the incoming solar flux. Even now there are no reproducible standards to measure absolute BRDFs to better than ±3%. Although the degradation of these diffusers in space are typically wavelength-dependent, reliable techniques [*Herman et al.*, 1991; *Bhartia et al.*, 1995] have been developed for determining the wavelength dependence but not the absolute degradation.

Figure 9 shows that the effect of a simple wavelength-independent radiance error on ozone profile can be quite complicated. The error pattern not only exhibits a strong altitude dependence but also varies with solar zenith angle, and to a smaller extent with the ozone profile itself. These results clearly show the desirability of correcting the basic measurements of the instruments rather than after-the-fact adjustment of the derived ozone profiles based on some statistical analysis of the data.

6.2. Forward Model Errors

Sources of error in forward model include error in Rayleigh scattering and ozone absorption coefficients, and error in estimating I_{msr} using the R^*, p^* concept and the table look-up procedure. Also, since total ozone is considered a measurement for the profile retrieval, its errors can be considered as part of the forward model error.

The Rayleigh scattering coefficients determine the pressure scale of the retrieved profiles, that is, 1% error in these coefficients translates directly into 1% error in pressure. The percentage error in derived layer ozone amount is then simply the percentage error in pressure multiplied by the ratio of atmosphere to ozone scale height. This ratio is relatively large in the upper stratosphere, where it varies from ~1.6 in summer to ~1.8 in winter, decreases to 1 near the ozone mixing ratio peak (5–10 mbar), and becomes less than 1 below. The Rayleigh scattering cross sections per molecule are probably known to better than ~1% [*Bates*, 1984]. *Penndorf* [1957] speculates that his recommended value for the number of molecules in a

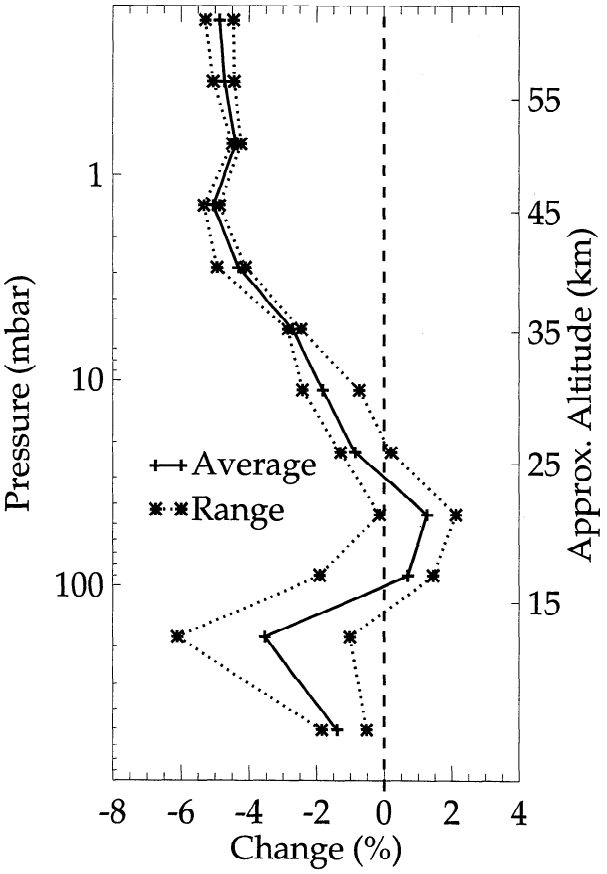

Figure 9. Effect of a 3% change in radiances at all wavelengths.

standard atmosphere (2.149×10^{25}), used for estimating β^* in Table 1, may vary by a "few percent" with atmospheric model. From the hydrostatic equation, the number of air molecules per unit pressure (Δn) is given by:

$$\Delta n = \frac{N_A}{Mg} \tag{12}$$

where, N_A is the Avogadro number, M is the molecular weight of air, and g is the acceleration due to gravity. Since Δn increases with altitude, z, as $[(R + z)/R]^2$, where R is Earth's radius, the number of molecules in one atmosphere column of air does vary with atmospheric model; but the variation from Penndorf's recommended value is only ~0.1%. The altitude dependence of Δn, however, introduces altitude dependence in β^*, which is not accounted for in calculating buv radiances from (1). The effect of this error is to cause ~2.5% underestimation of ozone near 50 km, reducing to less than 1% below 30 km.

Ozone absorption coefficients determine the ozone scale, that is, 1% error in these coefficients translate into 1% error in layer ozone amount or ozone mixing ratio. Errors in estimating these coefficients include errors in laboratory measurements of *Bass and Paur* [1984], errors in estimating the temperature at which these coefficients are calculated, and approximations made in computing band-averaged radiances using effective coefficients. At the profiling wavelengths the combined errors are ~1–2%.

A potential source of error in estimating I_{msr} is the validity of the assumption that R^* is wavelength independent. This assumption has been verified using the total ozone mapping spectrometer (TOMS) instrument that flew on the Nimbus 7 satellite with SBUV. TOMS has additional wavelengths, outside the ozone absorption band, that were specifically designed to study the wavelength dependence of R^*. Comparison of R^* derived from the measurements at 4 wavelengths (380, 360, 340, 331 nm) show that the concept of LER works reasonably well under a large variety of observing conditions. However, variations in R^* of up to ±0.001/nm are sometimes observed. For scenes containing partial or thin clouds, R^* is observed to increase with decrease in wavelength; while in the presence of sea glint, or when UV-absorbing aerosols (most commonly found in desert dust storms and near biomass burning regions) are present, R^* decreases with decreasing wavelength. These variations introduce about 1% rms. error in calculating the buv radiances at the longer buv wavelengths (>300 nm). The shorter buv wavelengths are usually not affected by these errors.

However, the concept of R^* breaks down when very high altitude (>22 km) aerosols produced after a major volcanic eruption are present in the stratosphere [*Bhartia et al.*, 1993]. Although these aerosols do not perturb the long wavelength radiation used in deriving R^* as much, they can cause a large increase in the buv radiances for wavelengths whose contribution functions peak near the altitude where the aerosols are present [*Torres and Bhartia*, 1995]. Since the aerosol effects are a strong function of not only the aerosol optical thickness but also the height of the aerosol layer, which is often not known very well, the current algorithm does not account for the effects of the volcanic aerosols in computing the buv radiances. These errors, however, are usually short-lived, typically lasting for only a few month to a year after a major volcanic eruption depending on the altitude of the aerosol layer. Although the data most severely contaminated by aerosols are flagged using an internal consistency check [*Fleig et al.*, 1990], the procedure misses low-level aerosol contamination [*Torres and Bhartia*, 1995].

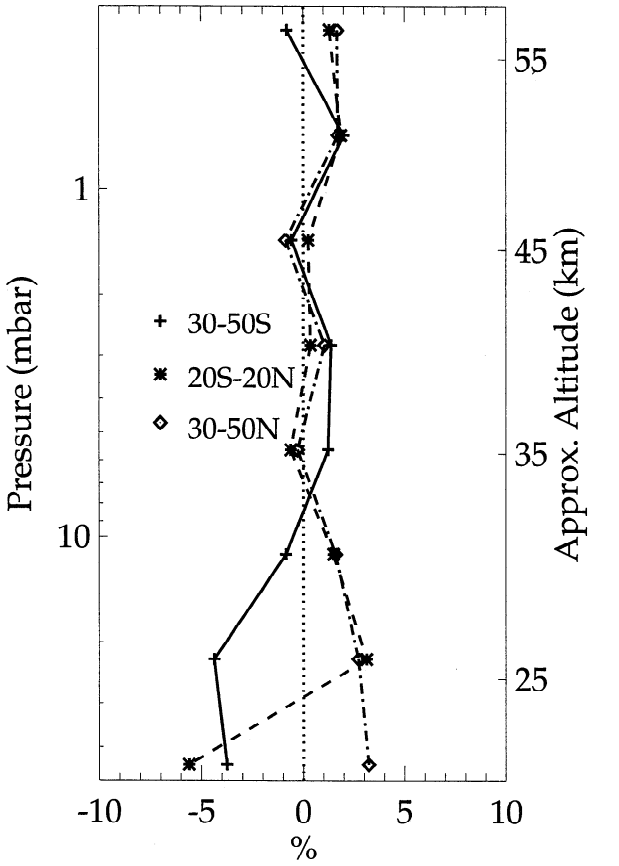

Figure 10. Change in rms error from assuming that the MSR component of the buv radiances were estimated perfectly, rather than the imperfect table look-up procedure used by the current algorithm.

Errors in p^* primarily occur at high reflectivities where the buv radiances are insensitive to Rayleigh scattering. Therefore, the primary effect of uncertainty in p^* is in estimating the ozone column below p^* which must be added to the measured ozone column above p^* to estimate the total column ozone. Since one only needs to know the ozone column above p^* to estimate the MSR component of the radiances used in profile inversion, uncertainty in p^* is not a significant error source for profiling.

Finally, we estimate the error in using the table look-up procedure by comparing the estimated MSR with exact calculation using simulated ozone profiles constructed from SAGE II data set. Both total and single-scattered radiances were computed by exact radiative transfer calculations, and then compared with the results from the table look-up procedure. Figure 10 shows the effect of this error on the derived ozone profiles. The primary effect is in the lower atmosphere where the inverse model errors discussed in the previous section are dominant. So, little is lost by using the table look-up procedure instead of direct, computer-intensive, calculation of MSR.

6.3. Inverse Model Errors

We define the inverse model errors as those errors that can be attributed solely to the process of inverting radiances to obtain a vertical ozone profile. These errors arise from the fact

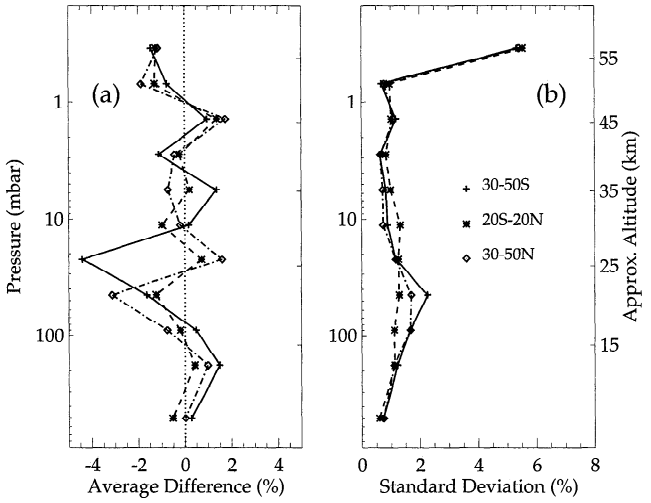

Figure 11. (a) Mean errors ((SBUV-SAGE)/SAGE) and (b) standard deviation of errors in retrieving cumulative ozone profiles constructed from 6 years of SAGE II data. Data are binned in three latitude bands where SAGE provides adequate seasonal coverage.

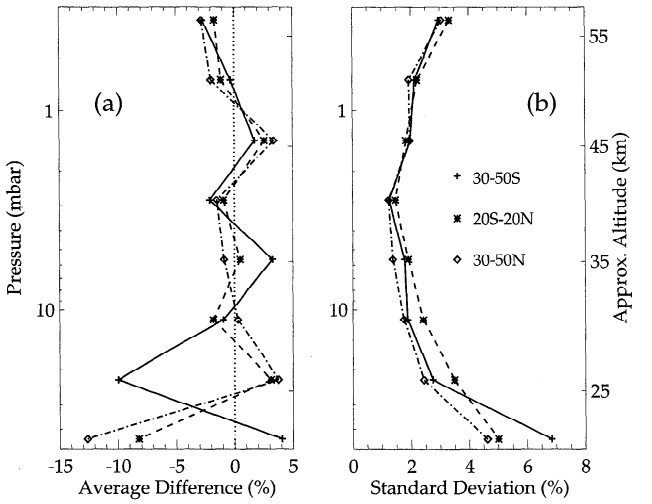

Figure 12. Same as in Figure 11, but for layer ozone amounts. Layers below four are not shown because of large enhancement in error (Figure 4).

that the inversion of buv radiances into an ozone profile requires a priori assumptions. At best, these a priori assumptions define the statistical properties of some selected ensemble of profiles. Therefore, even in the absence of measurement or forward model errors, any single retrieval or an ensemble average of profiles different from those represented by the a priori will have errors.

Direct comparison between SAGE II and SBUV derived ozone profiles have been made [*McPeters et al.*, 1994; *Rusch et al.*, 1994]. However, these comparisons fail to provide unambiguous answers about the capability of the buv inversion algorithm itself, for they are affected by spatial and temporal collocation errors, instrumental errors, and forward model errors of both instruments. In addition, as pointed out by *McPeters et al.* [1994] SAGE/SBUV comparisons are subject to errors in converting from altitude scale to pressure scale required for computing Umkehr layer ozone amounts from the SAGE ozone number density data. To avoid such problems, we consider how the buv algorithm would respond to buv radiances calculated directly from the SAGE profiles. Since neither the SAGE profiles nor the computed buv radiances are assumed to have errors, we are able to quantify the errors resulting purely from the buv inversion model itself. A similar technique was used by *DeLuisi et al.* [1989] to compare Umkehr and SBUV (version 5.0) algorithms.

As expected, the SAGE comparisons show that the buv technique can measure the cumulative ozone amounts above a pressure surface to a high degree of precision. Figure 11 shows that, in the absence of measurement errors, cumulative ozone profiles between the surface and 55 km are derived with a precision of better than 2%. Figure 12 shows the corresponding errors for layer ozone amounts. Lower layers are not shown since the percentage errors for these layers lose meaning because of (11). One notes that the errors do not average to zero when large number of profiles are averaged. This is a consequence of a priori constraint which may introduce systematic errors if the a priori profile is not the ensemble average of the subset of SAGE II data examined. This appears to be the case in the lower layers at southern midlatitudes. The results reported in Figure 12 are somewhat worse than reported by *DeLuisi et al.* [1989], for they used monthly mean SAGE II and ozonesonde profiles, while we use daily mean profiles that have far greater variability.

6.4. Overall Errors

The three types of errors discussed above have very different statistical properties. How one combines them together depends upon the intended application. For a single buv profile, the root sum of squares (RSS) of individual errors, given in Table 4, provides a reasonable estimate of errors. For zonal means, the random errors average out. So, the errors are dominated by systematic instrument calibration errors in the upper stratosphere, and by inverse model errors in the lower stratosphere. Both these errors may change in time, as the instrument drifts and as the ensemble average of profiles drift away from a priori due to geophysical variability. These errors must be estimated on a case-by-case basis. For the Nimbus 7 SBUV experiment, *Bhartia et al.* [1995] provide an estimated uncertainty due to calibration drift. The effect of inverse model errors on long-term trend is more difficult to quantify. One basically has two choices. If a trend estimate is available for another source (e.g., numerical models, ozonesondes, or other satellite instruments), one can estimate how the buv algorithm would respond to such changes. These results can then be compared with the actual data to see if the predicted and observed changes agree. In absence of such models, one is restricted to using the buv retrieved profiles between 1 and 20 mbar where the inverse model errors are small. Outside this range, only the cumulative ozone amounts (between 20 mbar and surface, and above 1 mbar) are relatively free of a priori assumptions to be suitable for long-term trends.

Finally, it should be mentioned that there are some applications for which one simply needs the cumulative ozone amounts above a pressure surface, rather than the layer ozone amounts or mixing ratios. These applications include estimation of ozone above the burst altitude of ozonesondes to obtain total column ozone [*McPeters et al.*, 1996] and estimation of stratospheric column ozone to derive tropospheric ozone residuals from total ozone measurements [*Fishman et al.*, 1986]. For these applications one should note that the cumulative

ozone from the buv technique can be obtained to a higher degree of accuracy, relatively free of a priori assumptions (Figure 11), than the ozone amounts in individual layers.

7. Conclusion

We have described the current operational version (Version 6.0) of the profile algorithm developed by NASA's Ozone Processing Team (OPT) for the processing of data from the buv instruments. The algorithm essentially retrieves a 12-node natural cubic spline curve in the logarithm of cumulative ozone versus the logarithm of pressure coordinate system. For the convenience of users, however, data are reported as column ozone in 12 roughly 5-km layers, similar to those used by Umkehr, and also as ozone mixing ratios at 19 standard pressures, obtained from the first derivative of the spline curve. Sixteen years of ozone data processed using this algorithm are now available from NASA and NOAA archives.

Simulation results using SAGE profiles indicate that the buv technique can capture large-scale variabilities of ozone over a broad range of atmosphere (0.3–100 mbar), with rms errors ranging from 5 to 15%. However, over part of this range the results are heavily influenced by the a priori assumptions. SAGE results essentially confirm the validity of these assumptions, thus making it possible to use the buv technique to extend the limited spatial and temporal coverage of SAGE for the studies of latitudinal, seasonal, and planetary scale variabilities. This, however, does not imply that buv profile data over the entire 0.3 to 100 mbar range are reliable for all studies. Response of the algorithm to ozone impulse applied at different altitudes indicates that for those studies where the a priori assumptions are not necessarily valid, for example, long-term trends, one should restrict the analysis to between 1 and 20 mbar (30–50 km), where the dependence on a priori is small. Outside this region, only the column amounts (between 20 mbar and surface, and above 1 mbar) can be considered to be relatively free of a priori assumptions.

References

Bass, A. M. and R. J. Paur, The ultraviolet cross-section of ozone, I, The measurements, in *Atmospheric Ozone*, edited by C. S. Zerefos and A. Ghazi, pp. 606–610, D. Reidel, Norwood, Mass., 1984.

Bates, D. R., Rayleigh scattering by air, *Planet. Space Sci., 32*, 785–790, 1984.

Bhartia, P. K., K. F. Klenk, A. J. Fleig, R. D. McPeters, and C. L. Mateer, Algorithm for vertical ozone profile determination from the Nimbus 4 BUV dataset, in *Fourth Conference on Atmospheric Radiation*, Am. Meteorol. Soc., Boston, Mass., 1981.

Bhartia, P. K., J. Herman, R. D. McPeters, and O. Torres, Effect of Mount Pinatubo aerosols on total ozone measurements from backscatter ultraviolet (BUV) experiments, *J. Geophys. Res., 98*, 18,547–18,554, 1993.

Bhartia, P. K., S. Taylor, R. McPeters, and C. Wellemeyer, Application of the Langley Plot method to the calibration of SBUV instrument on Nimbus-7 satellite, *J. Geophys. Res., 100*, 2997–3004, 1995.

Caudill, T. R., Accuracy of the Total Ozone Mapping Spectrometer algorithm at polar latitudes, Ph.D. dissertation, Univ. of Ariz., Tucson, 1994.

Cebula, R. P., H. Park, and D. F. Heath, Characterization of the Nimbus-7 SBUV radiometer for the long-term monitoring of the stratospheric ozone, *J. Atmos. Oceanic Tech., 5*, 215–227, 1988.

Dave, J. V., Meaning of successive iteration of the auxiliary equation of radiative transfer, *Astrophys. J., 140*, 1292–1303, 1964.

Dave, J. V., Investigation of the effect of atmospheric dust on the determination of total ozone from the earth's ultraviolet reflectivity measurements, *NTIS Accession 77-24690–24692*, Int. Bus. Mach. Corp., Gaithersburg, Md, 1977.

Dave, J. V., and C. L. Mateer, A preliminary study on the possibility of estimating total atmospheric ozone from satellite measurements, *J. Atmos. Sci., 24*, 414–427, 1967.

DeLuisi, J. J., D. U. Longenecker, P. K. Bhartia, S. Taylor, and C. L. Mateer, Ozone profiles by Umkehr, SBUV, and ozonesonde: A comparison including the inversion algorithms for Umkehr and SBUV, in *Ozone in the Atmosphere*, edited by R. D. Bojkov and P. Fabian, pp. 206–210, A. Deepak, Hampton, Va., 1989.

Fishman, J., P. Minnis, J. Henry, and G. Reichle, Use of satellite data to study tropospheric ozone in the tropics, *J. Geophys. Res., 91*, 14,451–14,465, 1986.

Fitzmaurice, J. A., Simplification of the Chapman Function for atmospheric attenuation, *Appl. Opt., 3*, 640, 1964.

Fleig, A. J., R. D. McPeters, P. K. Bhartia, B. M. Schlesinger, R. P. Cebula, K. F. Klenk, S. L. Taylor, and D. F. Heath, Nimbus 7 Solar Backscatter Ultraviolet (SBUV) ozone products user's guide, *Rep.* NASA RP-1234, Natl. Aeronaut. and Space Admin., Goddard Space Flight Cent., Greenbelt, Md., 1990.

Heath, D. F., A. J. Krueger, H. R. Roeder, and B. D. Henderson, The Solar Backscatter Ultraviolet and Total Ozone Mapping Spectrometer (SBUV/TOMS) for Nimbus G, *Opt. Eng., 14*, 323–331, 1975.

Heath, D. F., A. J. Krueger, and H. Park, The Solar Backscatter Ultraviolet (SBUV) and Total-Ozone Mapping Spectrometer (TOMS) Experiment, in *The Nimbus 7 User's Guide*, edited by C. R. Madrid, pp. 175–211, NASA Goddard Space Flight Center, Greenbelt, Md., 1978.

Herman, J. R., R. Hudson, R. McPeters, R. Stolarski, Z. Ahmad, X. Y. Gu, S. Taylor, and C. Wellemeyer, A new self-calibration method applied to TOMS and SBUV backscattered ultraviolet data to determine long-term global ozone changes, *J. Geophys. Res., 96*, 7531–7545, 1991.

Hilsenrath, E., D. E. Williams, R. T. Caffrey, R. P. Cebula, and S. J. Hynes, Calibration and radiometric stability of the Shuttle Solar Backscatter Ultraviolet (SSBUV) experiment, *Metrologia, 30*, 243–248, 1993.

Hilsenrath, E., R. P. Cebula, M. T. Deland, K. Laamann, S. Taylor, C. Wellemeyer, and P. K. Bhartia, Calibration of the NOAA 11 solar backscatter ultraviolet (SBUV/2) ozone data set from 1989 to 1993 using in-flight calibration data and SSBUV, *J. Geophys. Res., 100*, 1351–1366, 1995.

Hudson, R. D., J. Kim, and A. M. Thompson, On the derivation of tropospheric column ozone from radiances measured by the Total Ozone Mapping Spectrometer, *J. Geophys. Res., 100*, 11,137–11,145, 1995.

Klenk, K. F., Absorption coefficients of ozone for the backscatter UV experiment, *Appl. Opt., 19*, 236–242, 1980.

Klenk, K. F., P. K. Bhartia, A. J. Fleig, V. G. Kaveeshwar, R. D. McPeters, and P. M. Smith, Total ozone determination from the Backscattered Ultraviolet (BUV) experiment, *J. Appl. Meteorol., 21*, 1672–1684, 1982.

Klenk, K. F., P. K. Bhartia, A. J. Fleig, and C. L. Mateer, Vertical ozone profile determination from Nimbus-7 SBUV measurements, in *Fifth Conference on Atmospheric Radiation*, Am. Meteorol. Soc., Boston, Mass., 1983.

Krueger, A. J., D. F. Heath, and C. L. Mateer, Variations in the stratospheric ozone field inferred from Nimbus satellite observations, *Pure Appl. Geophys., 106*, 1254–1263, 1973.

Mateer, C. L., A review of some aspects of inferring the ozone profile by inversion of ultraviolet radiance measurements, in *Mathematics of Profile Inversion*, edited by L. Colin, NASA Ames Res. Cent., Moffett Field, Calif., 1971.

Mateer, C. L., and J. J. DeLuisi, A new Umkehr inversion algorithm, *J. Atmos. Terr. Phys., 54*, 537–556, 1992.

Mateer, C. L., D. F. Heath, and A. J. Krueger, Estimation of total ozone from satellite measurements of backscattered ultraviolet Earth radiance, *J. Atmos. Sci., 28*, 1307–1311, 1971.

McCormick, M. P., J. M. Zawdodny, R. E. Veiga, J. C. Larsen, and P. H. Wong, An oversview of SAGE I and II ozone measurements, *Planet. Space Sci., 37*, 1567–1586, 1989.

McPeters, R. D., The behavior of ozone near the stratopause from 2 years of BUV observations, *J. Geophys. Res., 85*, 4545–4550, 1980.

McPeters, R. D., Climatology of Nitric Oxide in the upper stratosphere, mesosphere, and thermosphere: 1979 through 1986, *J. Geophys. Res., 94*, 3461–3472, 1989.

McPeters, R. D., et. al., Nimbus 7 Total Ozone Mapping Spectrometer

(TOMS) data products user's guide, Rep. NASA RP-1323, Natl. Aeronaut. and Space Admin., Greenbelt, Md., 1993.

McPeters, R. D., T. Miles, L. E. Flynn, C. G. Wellemeyer, and J. M. Zawodny, Comparison of SBUV and SAGE II ozone profiles: Implications for ozone trends, *J. Geophys. Res.*, *99*, 20,513–20,524, 1994.

McPeters, R. D., G. J. Labow, and B. J. Johnson, An SBUV ozone climatology for balloonsonde estimation of total column ozone, *J. Geophys. Res.*, in press, 1996.

Penndorf, R., Tables of the refractive index for standard air and the Rayleigh scattering coefficient for the spectral region between 0.2 and 20.0μ and their application to atmospheric optics, *J. Opt. Soc. Am.*, *47*, 176–182, 1957.

Rawcliffe, R. D., and D. D. Elliott, Latitude distribution of ozone at high altitudes, deduced from a satellite measurement of the Earth's radiance at 2840A, *J. Geophys. Res.*, *71*, 5077–5089, 1966.

Rodgers, C. D., Retrieval of atmospheric temperature and composition from remote measurements of thermal radiations, *Rev. Geophys.*, *14*, 609–624, 1976.

Rodgers, C. D., Characterization and error analysis of profiles retrieved from remote sounding measurements, *J. Geophys. Res.*, *95*, 5587–5595, 1990.

Rusch, D. W., R. T. Clancy, and P. K. Bhartia, Comparison of satellite measurements of ozone and ozone trends, *J. Geophys. Res.*, *99*, 20,501–20,511, 1994.

Thomas, R. W. L., and A. C. Holland, Simple relationship between the UV radiation backscattered by the Earth's atmosphere and the vertical ozone profile, *Appl. Opt.*, *16*, 2581–2583, 1977.

Torres, O., and P. K. Bhartia, Effect of stratospheric aerosols on ozone vertical profiles derived from the backscatter ultraviolet (BUV) technique, *Geophys. Res. Lett.*, *22*, 235–238, 1995.

Twomey, S., On the numerical solution of Fredholm integral equations of the first kind by the inversion of the linear systems produced by quadrature, *J. Assoc. Comput. Mach.*, *10*, 97–101, 1963.

Weiss, H., R. P. Cebula, and K. Laamann, Evaluation of the NOAA-11 Solar Backscatter Ultraviolet Radiometer, Mod 2 (SBUV/2) inflight calibration, in *Calibration of Passive Remote Observing Optical and Microwave Instrumentation*, SPIE, Orlando, Florida, 1991.

World Meteorological Organization (WMO), Report of the international ozone trends panel, *18*, World Meteorol. Org., Geneva, Switzerland, 1988.

Yarger, D. N., An evaluation of some methods of estimating the vertical atmospheric ozone distribution from the inversion of spectral ultraviolet radiation, *J. Appl. Meteorol.*, *9*, 921–928, 1970.

P. K. Bhartia and R. D. McPeters, Mail Code 916, NASA/Goddard Space Flight Center, Greenbelt, MD 20771. (Bhartia@chapman.gsfc.nasa.gov)

L. E. Flynn, Software Corporation of America, 4601 Presidents Drive, Suite 350, Lanham, MD 20706.

C. L. Mateer, 1210-255 Bamburgh Circle, Scarborough, ONT. Canada

C. Wellemeyer, Hughes STX Corporation, 7701 Greenbelt Road, Greenbelt, MD 20770.

(Received July 11, 1995; revised March 8, 1996;
accepted March 28, 1996.)